

Distribution Agreement

In presenting this thesis as a partial fulfillment of the requirements for a degree from Emory University, I hereby grant to Emory University and its agents the non-exclusive license to archive, make accessible, and display my thesis in whole or in part in all forms of media, now or hereafter now, including display on the World Wide Web. I understand that I may select some access restrictions as part of the online submission of this thesis. I retain all ownership rights to the copyright of the thesis. I also retain the right to use in future works (such as articles or books) all or part of this thesis

Daniel Cristian Salgueiro

March 26, 2018

Kinetic Studies of Rhodium(III)-Catalyzed Allylic C-H Amination of Disubstituted Olefins

By

Daniel Cristian Salgueiro

Simon B. Blakey, Ph.D.

Advisor

Department of Chemistry

Simon B. Blakey, Ph.D.

Advisor

Cora E. MacBeth, Ph.D.

Committee Member

Arri Eisen, Ph.D.

Committee Member

2018

Kinetic Studies of Rhodium(III)-Catalyzed Allylic C-H Amination of Disubstituted Olefins

By

Daniel Cristian Salgueiro

Simon B. Blakey, Ph.D.

Advisor

An abstract of

A thesis submitted to the Faculty of Emory College of Arts and Sciences
of Emory University in partial fulfillment
of the requirements of the degree of
Bachelor of Sciences with Honors

Department of Chemistry

2018

Abstract

Kinetic Studies of Rhodium(III)-Catalyzed Allylic C-H Amination of Disubstituted Olefins

By Daniel Cristian Salgueiro

Allylic substitution reactions have been a powerful tool used by synthetic chemists since the 1960s and 1970s. Traditional allylic substitution reactions have required pre-functionalized olefins and stoichiometric equivalents of transition metals to generate the desired product. The Blakey lab has recently developed methodology for the rhodium (III)-catalyzed allylic C-H amination of 1,2-disubstituted alkenes that is tolerant of a broad array of amine nucleophiles and aryl, alkyl alkenes. However, the complete mechanism of this transformation remains unknown. We have performed kinetics studies on the allylic C-H amination of 1,3-diphenyl propene with benzyl carbamate as the nucleophile and have determined that this reaction proceeds in an overall pseudo-zero order fashion and that the reaction exhibits first order dependence on both rhodium and alkene, and is inhibited by the amine nucleophile. Based on kinetic studies, stoichiometric reactions with rhodium π -allyl complexes, and collaborations with computational chemists we propose that the reaction requires both an oxidant and a carboxylate source, and that it may proceed through a $\text{Rh}^{\text{II}}/\text{Rh}^{\text{IV}}$ catalytic cycle.

Kinetic Studies of Rhodium(III)-Catalyzed Allylic C-H Amination of Disubstituted Olefins

By

Daniel Cristian Salgueiro

Simon B. Blakey, Ph.D.

Advisor

A thesis submitted to the Faculty of Emory College of Arts and Sciences
of Emory University in partial fulfillment
of the requirements of the degree of
Bachelor of Sciences with Honors

Department of Chemistry

2018

Acknowledgements

I would first like to thank Dr. Simon Blakey for all his guidance and support both in and outside the lab. My time in the Blakey lab has helped me grow from a clueless undergraduate student into a somewhat competent scientist.

I thank Dr. Cora MacBeth for her general guidance and advice throughout my undergraduate career. Dr. MacBeth was always more than willing to offer advice and support even with her busy schedule as both a professor and a dean.

I would also like to thank Dr. Arri Eisen who taught both my first and last class at Emory. Dr. Eisen has helped me view science through a different lens, and taught me so much along the way

The work in this thesis could not have been done without the guidance and input from Dr. Robert Harris, the training from Taylor Nelson, and the input of Jacob Burman. I also want to thank my family, my friends, and everyone in the MacBlakey super group. I cannot even imagine what my time at Emory would have been like without the support and encouragement from all these people, and I will be sad to leave Emory in May.

Table of Contents

Introduction	1
Results and Discussion	7
I. Kinetics	7
II. Oxidant Screening	10
III. Controls (Role of Carboxylates)	11
IV. Stoichiometric π -allyl Complex Reactions	12
V. Computational Studies	13
Conclusions and Future Directions	19
Supplemental Information	20
References	38
Figures	
Figure 1: Historical approaches for allylic functionalization via the generation of metal π -allyl intermediates	1
Figure 2: Precedence for allylic C–H functionalization of terminal olefins	3
Figure 3: Allylic C–H Functionalizations of internal olefins with Rh(III)Cp* on ω -unsaturated <i>N</i> -sulfonylamines	4
Figure 4: Generation and reactivity of rhodium π -allyl complexes	5
Figure 5: Representation of inner sphere and outer sphere pathways for allylic C–H amination	6
Figure 6: Representative Kinetic Plot	8
Figure 7: . Catalyst concentration dependence of the rate of the amination of 1	9
Figure 8: [1] dependence of the rate of the amination of 1	9
Figure 9: [2] dependence of the rate of the amination of 1	10
Figure 10: Oxidants tested for solubility and viability under reaction conditions	11
Figure 11: Stoichiometric amination of Rh π -allyl complex 4	13

Figure 12: Computational studies depicting one possible pathway for the Rh ^{II} /Rh ^{IV} catalyzed allylic C–H amination of alkene 1	14
Figure 13: Computational studies depicting one possible pathway for the Rh ^I /Rh ^{III} catalyzed allylic C–H amination of alkene 1	15
Figure S1: GC-FID of 1,3-diphenyl propene	28
Figure S2: GC-FID of benzyl carbamate	28
Figure S3: GC-FID of aminated product 3	28
Figure S4: GC-FID of the internal standard	29
Figure S5: GC-FID of a running reaction as described in the kinetics studies procedure	29
Figure S6: A representative plot of product formation over time under reaction conditions shown in Scheme 1	32
Tables	
Table 1: Reaction screen with monomeric rhodium pre-catalysts	12
Table 2: Reactions with isolated Rh π -allyl complex 4	13
Table S1: Response factors of kinetically relevant species and response factor ratios relative to nonane	32
Table S2: Global reaction rate dependence on [Rh catalyst]	33
Table S3: Global reaction rate dependence on [olefin]	34
Table S4: Global reaction rate dependence on [nucleophile]	34
Table S5: Global reaction rate dependence on [nucleophile]	34
Table S6: Global reaction rate dependence on [Halide Scavenger]	35
Table S7: Oxidant screening reactions	36
Table S8: Reaction screen with monomeric rhodium pre-catalysts	37
Schemes	

Scheme 1: Allylic C–H Amination with <i>p</i> -toluenesulfonamide	7
Scheme 2: Allylic C–H Amination with benzyl carbamate	7
Scheme 3: Proposed reaction mechanism	16
Scheme 4: Pre-equilibrium and rate determining step	16

Introduction

Allylic substitution reactions have been a widely used way of introducing complexity and additional functionality into simple, feedstock olefins since Tsuji and Trost pioneered this chemistry in the late 1960s and 1970s.¹ Traditionally, these reactions have required a transition metal catalyst and olefins with an allylic leaving group to generate a π -allyl intermediate, which can then be intercepted by a broad array of nucleophiles allowing for the formation of C–C, C–N, and C–O bonds in the allylic position.¹ More recently, π -allyl intermediates have been generated from alkynes or otherwise pre-oxidized olefins (Figure 1).^{2,3} Although this chemistry is quite robust, it is not an atom economical process due to the generation of a stoichiometric byproduct. Contemporary researchers have aimed to improve upon the Tsuji-Trost chemistry by setting out to accomplish the same transformations via metal-catalyzed C–H functionalization.

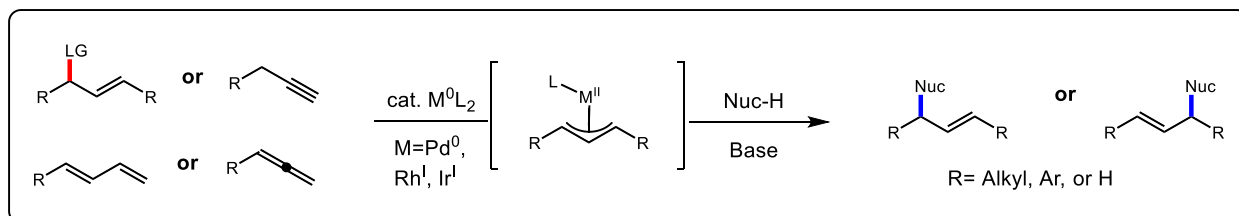


Figure 1. Historical approaches for allylic functionalization via the generation of metal π -allyl intermediates

As synthetic chemists interested in methodology, we aim to develop the ideal reaction. While previous methodologies required the use of leaving groups or otherwise pre-oxidized olefins, this work and future work strives to improve the state of C–H functionalization to make large scale industrial reactions greener and less wasteful. There are a number of natural products in which the synthetic route involves an allylic substitution reaction, and generating the pre-oxidized olefins needed for older methodologies adds more steps to the reaction, making it less efficient and more expensive to replicate.^{4,5} Circumventing these unnecessary steps via C–H

functionalization will allow for cheaper and more efficient synthesis of many natural products and relevant pharmaceuticals, which could drive down their cost and make lifesaving drugs more available to those who need them.

Early attempts at allylic C–H functionalization of unactivated olefins required the use of stoichiometric amounts of palladium to generate a palladium π -allyl intermediate, via a *syn*-hydride transfer, which can then react with the desired nucleophile.⁶ Initially, the effectiveness of catalytic C–H functionalization on these systems was limited because reaction conditions needed to support both the electrophilic C–H cleavage and oxidation of Pd⁰ necessary to drive the Pd catalyst back into the catalytic cycle. The White group has been able to overcome this challenge by using catalytic amounts of palladium with a bidentate bisulfonate ligand and stoichiometric benzoquinone as an oxidant (Figure 2).⁷ With this methodology in place, the White group used acetates, malonate type nucleophiles, and electron deficient amine nucleophiles to efficiently construct C–C, C–N, and C–O bonds from terminal olefins.⁸⁻¹⁰ The amination methodology is effective for C–H functionalization both intramolecularly and intermolecularly, however the reactions require the use of either tosyl-carbamates or triflyl amines as the nucleophile, the reaction is limited to terminal olefins, and the products of the reaction are difficult to deprotect to generate the free amine.

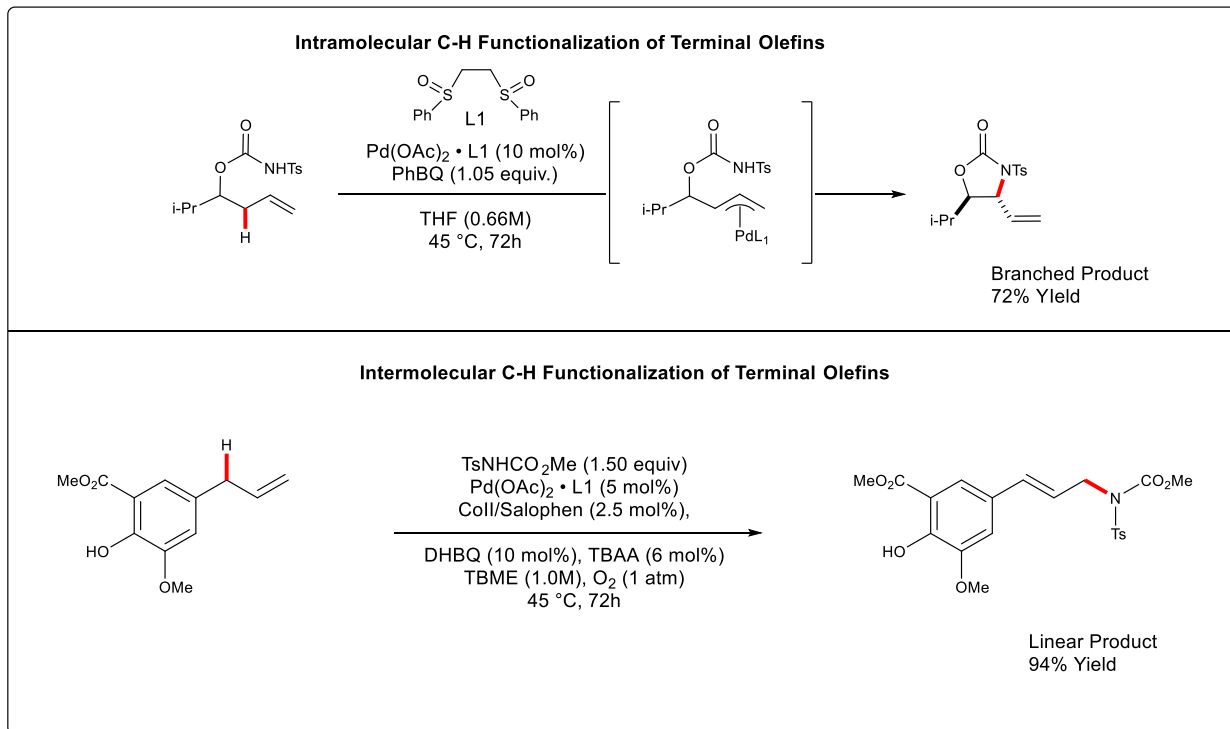


Figure 2. Precedence for allylic C–H functionalization of terminal olefins

The Cossy group has expanded on this transformation with the use of a rhodium(III)-pentamethylcyclopentadienyl complex to catalyze the C–H functionalization, which allows for the modification of the nucleophile for amination (Figure 3).¹¹ Additionally, this reaction was tolerant of both terminal and internal olefins. Unlike previously developed methodology, this transformation is tolerant of alkyl amines bearing only one electron withdrawing group and allows for C–H amination of both terminal olefins and 1,2-disubstituted olefins. While this methodology does allow for the use of singly-protected amine nucleophiles, it is limited to intramolecular amination.

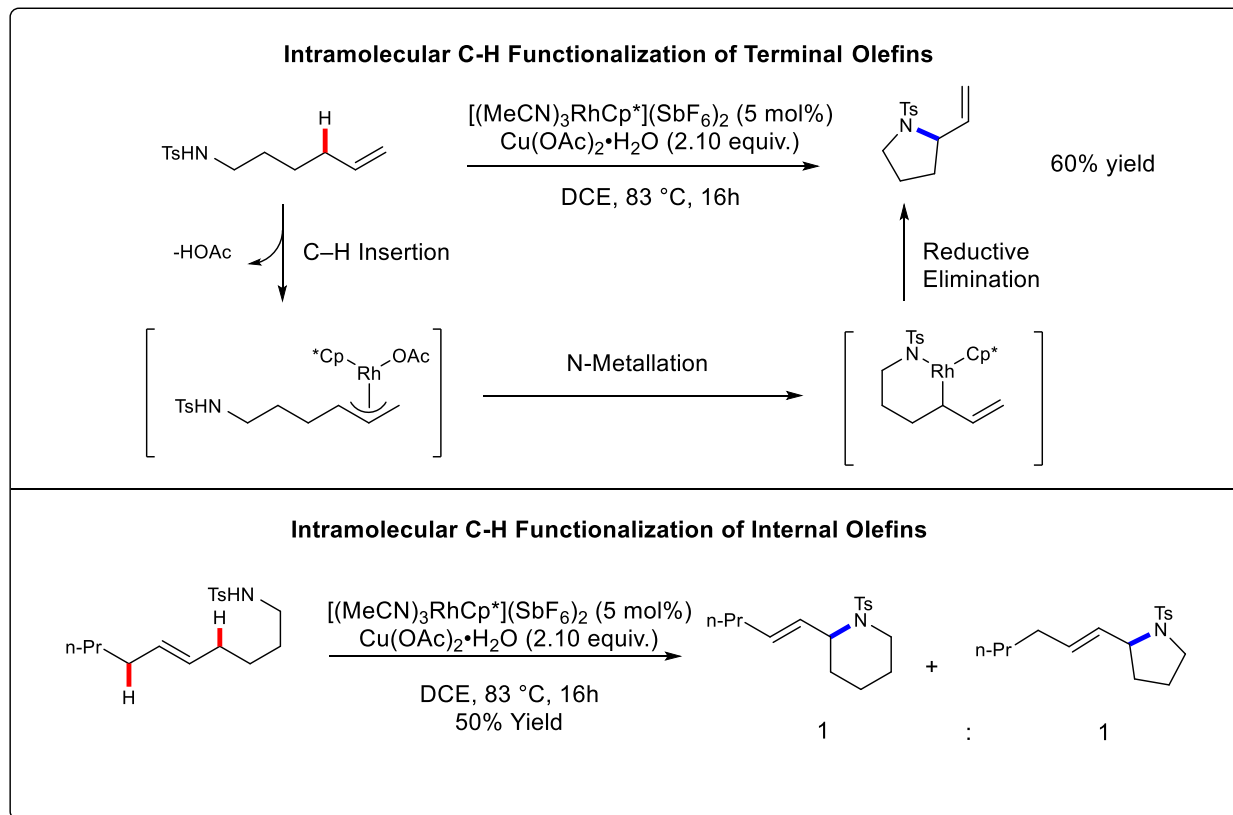


Figure 3. Allylic C–H Functionalizations of internal olefins with Rh(III)Cp* on ω -unsaturated *N*-sulfonylamines

The development of the electron deficient Cp^E ligand by the Tanaka group enabled the isolation of the postulated rhodium π -allyl complex (Figure 4).¹²⁻¹⁴ The Tanaka group then subjected these isolated π -allyl complexes to the reaction conditions reported by Cossy and generated the desired aminated product (Figure 4a), further supporting that this transformation proceeds via a π -allyl intermediate. Surprisingly, the formation of the new C–N bond occurs only in the presence of the Cu(OAc)₂. Interestingly, the rhodium π -allyl complexes generated from *trans*-2-octene favored the formation of an internal π -allyl complex as the major regioisomer. This result supports the idea that the reactivity of rhodium catalysts can be tuned to functionalize both terminal and internal olefins. These results support that rhodium cyclopentadienyl complexes may

be proficient catalysts for the intermolecular functionalization of allylic C–H bonds on 1,2-disubstituted olefins.

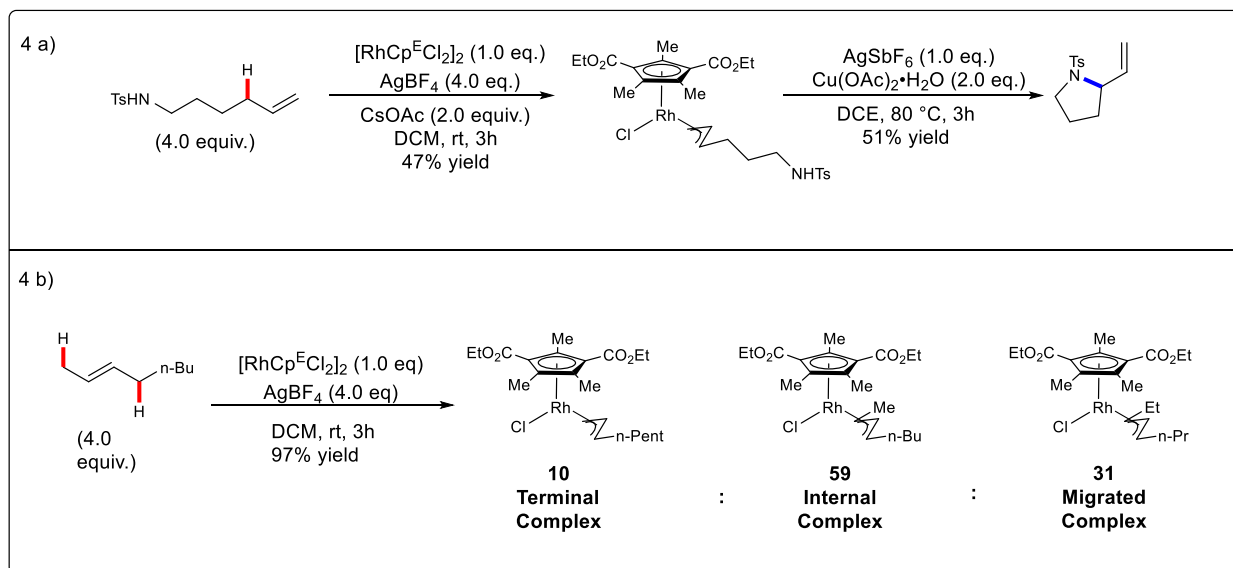


Figure 4. Generation and reactivity of rhodium π -allyl complexes

To this end, the Blakey group has recently developed methodology for a rhodium(III)-catalyzed intermolecular allylic C–H amination of 1,2-disubstituted olefins.¹⁵ This system tolerates a variety of aryl alkenes and a broad range of amine nucleophiles bearing only one electron-withdrawing group. Preliminary mechanistic investigations of this transformation reveal that the C–H cleavage step is irreversible while C–N bond may be reversible. However, the complete mechanism of this transformation is unknown, therefore probing the mechanism may provide insight for the development of new allylic C–H functionalization reactions.

Two mechanisms for the transition metal catalyzed allylic C–H amination have been proposed: innersphere and outersphere.⁹ An outer sphere mechanism would involve the formation of a rhodium π -allyl intermediate, which could then be subjected to nucleophilic attack, which would form the desired bond in the allylic position, regenerate the alkene, and the metal would subsequently dissociate from the aminated product. The second possibility is an inner sphere

mechanism like the one proposed by Cossy.¹¹ In this mechanism, after formation of the π -allyl species, the amine nucleophile would coordinate to the metal center, and a reductive elimination would then occur to afford the desired product.

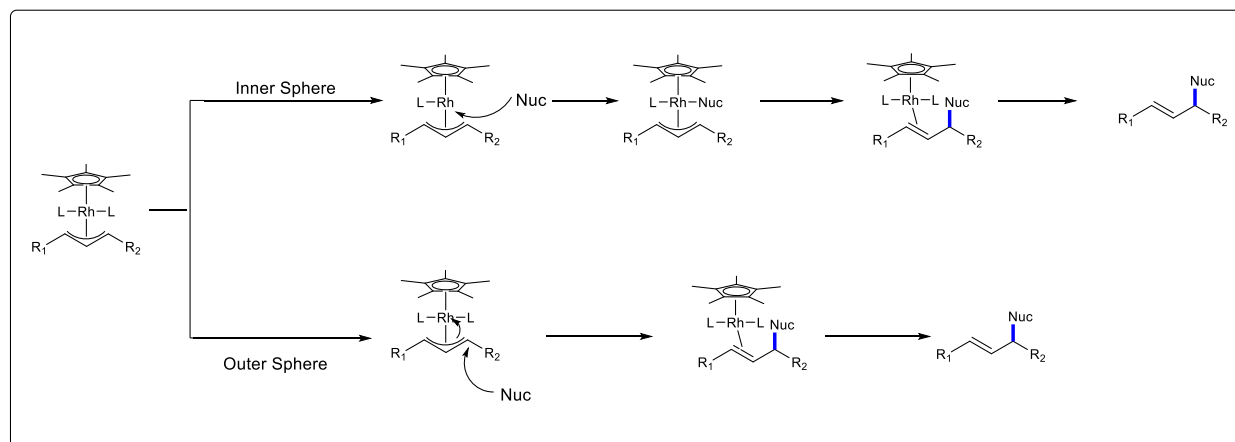


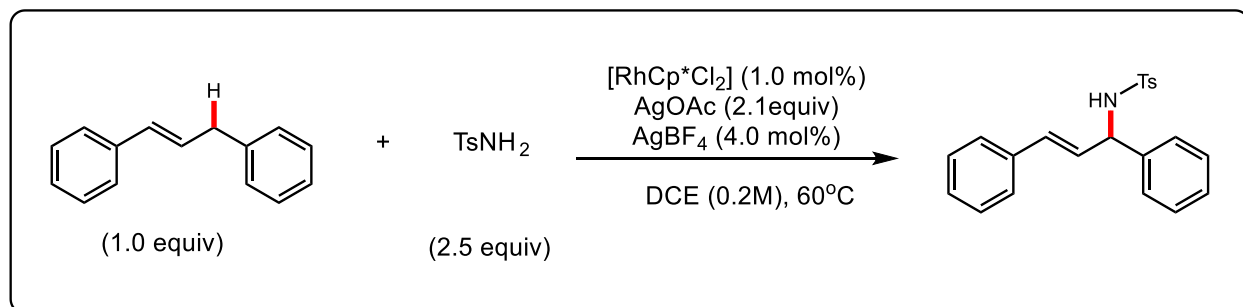
Figure 5. Representation of inner sphere and outer sphere pathways for allylic C–H amination.

Current efforts in the Blakey lab aim to move beyond allylic C–H amination, and methods have been developed to use these conditions to form C–O and C–C bonds as well. Understanding the mechanism of this transformation could allow for expansion of this chemistry into systems that are more difficult to access: selective functionalization of alkyl, alkyl alkenes, more highly substituted olefins, alkenes alpha to heteroatoms, and cyclic alkenes. Kinetic analysis of a reaction can provide extensive, indirect information on kinetically relevant intermediates, the nature of the catalytic resting state, and the molecules and intermediates involved in the rate determining step.¹⁶ Herein, we report the ongoing kinetic analysis of the rhodium catalyzed allylic C–H amination of 1,3-diphenyl propene with benzyl carbamate.

Results and Discussion

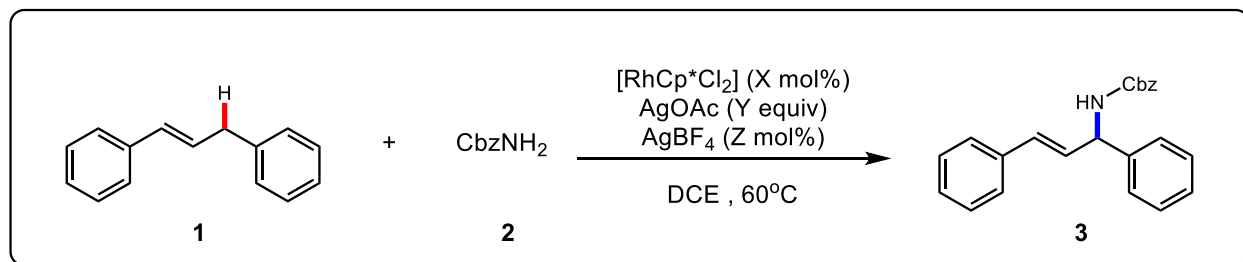
Kinetics

Scheme 1. Allylic C–H Amination with *p*-toluenesulfonamide



Because optimization studies identified 1,3-diphenyl propene and *p*-toluenesulfonamide (TsNH₂) as the combination of substrates that generated the highest yield for the reaction (Scheme 1), initial kinetic analysis focused on these starting materials. Additionally, utilizing an achiral nucleophile and an olefin that generates a symmetric π -allyl complex removes the extra complications of having to account for the formation of diastereomers and regioisomers. However, due to issues to the insolubility of TsNH₂ in DCE and complications with the work up of GC samples, interpreting kinetic data is difficult.

Scheme 2. Allylic C–H Amination with benzyl carbamate



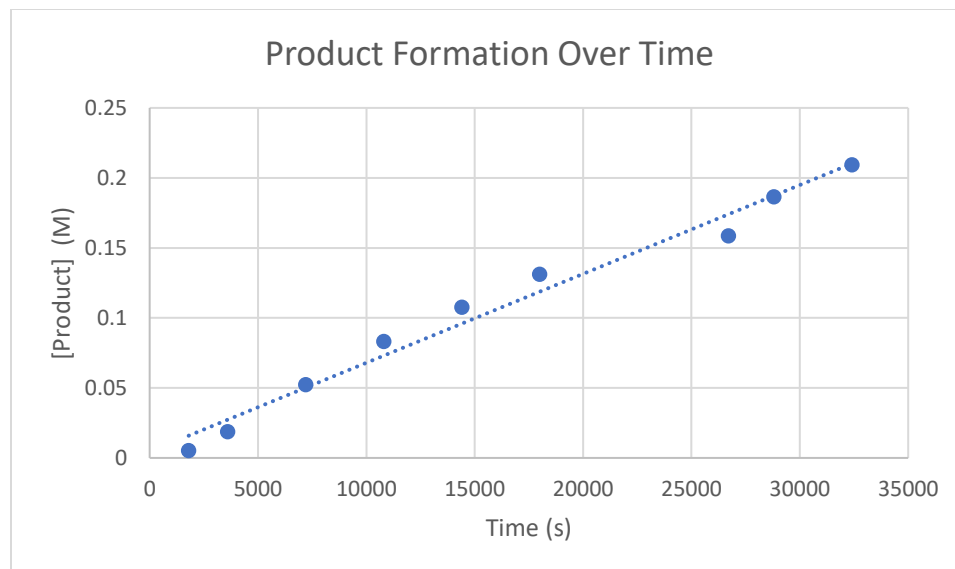


Figure 6. A representative plot of product formation over time with benzyl carbamate as the nucleophile

Switching to the more soluble benzyl carbamate (CbzNH_2), provided more straight forward kinetic data. In an initial experiment, a solution of **1** (0.2 M), **2** (0.5 M), AgOAc (0.42 M), AgBF_4 (0.024 M), and $[\text{RhCp}^*\text{Cl}_2]_2$ (0.006 M) in DCE at 60°C was monitored periodically by HPLC. A plot of **3** versus time was linear to greater than three half-lives with a pseudo zero order rate constant of $4.2 \pm 0.2 \times 10^{-6} \text{ M/s}$ (Table S2, Entry 4). From the graph in Figure 6 it is clear that the rate of product formation does not change over the course of the reaction, therefore the reaction proceeds in an overall pseudo-zero order manner.

Having established the overall pseudo zero order formation of product **3** over time, we set out to probe the order in each of the individual reactants. To accomplish this, the initial concentrations of reactants were varied to see their effect on the overall rate of the reaction. To determine the rate dependence on rhodium, pseudo-zero-order rate constants for the appearance of **3** as a function of $[[\text{RhCp}^*\text{Cl}_2]_2]$ from 0 to 0.008 M (Figure 7). A plot of the observed rate versus $[[\text{RhCp}^*\text{Cl}_2]_2]$ was linear, which established first order dependence of the rate of amination

of **1** with **2** on catalyst concentration with a pseudo-first-order rate constant of $k_1 = 7.9 \pm 0.8 \times 10^{-4} \text{ s}^{-1}$

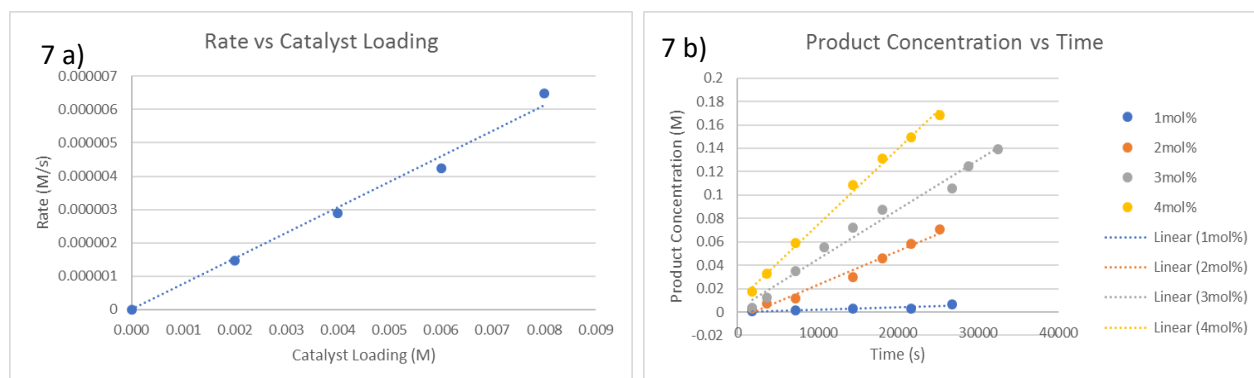


Figure 7. Catalyst concentration dependence of the rate of the amination of **1** (0.2 M) with **2** (0.5 M), AgOAc (0.42 M), AgBF₄ (0.024 M) catalyzed by [RhCp*Cl₂]₂ (0-0.008 M) in DCE at 60°C.

To determine the rate dependence on olefin concentration, the rates were determined as a function of [**1**] from 0 to 0.5 M. A plot of the observed rate versus [**1**] was linear (Figure 8), which established the first-order dependence of the rate of amination of **1** with **2** on olefin **1** concentration with a pseudo-first-order rate constant of $k_1 = 1.60 \pm 0.04 \times 10^{-5} \text{ s}^{-1}$.

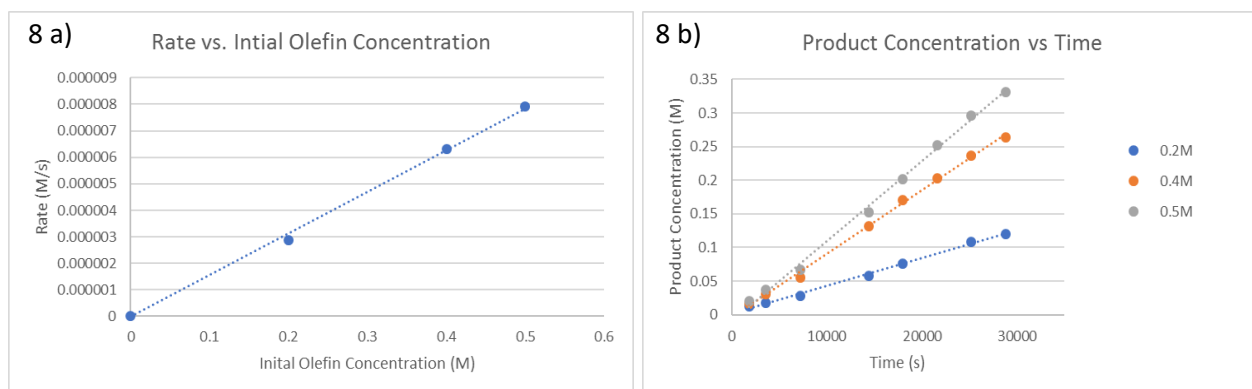


Figure 8. [**1**] dependence of the rate of the amination of **1** (0-0.5 M) with **2** (0.5 M), AgOAc (0.42 M), and AgBF₄ (0.024 M), catalyzed by [RhCp*Cl₂]₂ (0.006 M) in DCE at 60°C global rate of the reaction plotted as a function of initial concentration of olefin **1**

To determine the rate dependence on amine concentration, the observed rates were determined as a function of [2] from 0.25 to 1.0 M (Figure 9). A plot of the observed rate versus [2] had an overall downward trend, meaning that amine 2 inhibits the formation of product 3. This inhibition of product formation may stem from the ability of 2 to coordinate to the rhodium center and bring it into an off-cycle resting state.

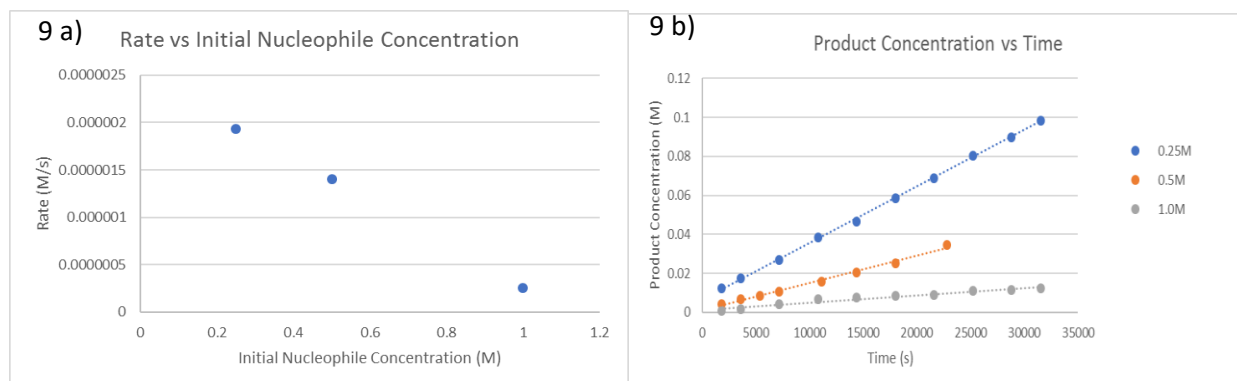


Figure 9. [2] dependence of the rate of the amination of 1 (0.2 M) with 2 (0.25-1.0 M), AgOAc (0.42 M), and AgBF₄ (0.024 M), catalyzed by [RhCp*Cl₂]₂ (0.002 M) in DCE at 60°C global rate of the reaction plotted as a function of initial concentration of amine 2.

Reactions carried out with varying concentrations of silver tetrafluoroborate suggest that this silver salt is necessary for abstracting the halides from rhodium to generate an active catalyst, but adding more equivalents does not increase the global rate of the reaction, signifying a zero order dependence. The addition of 50 mol% of the aminated product to a reaction under standard conditions revealed that there is no significant rate inhibition caused by the product. Additionally, the lack of change in reaction rate shows that the catalyst does not decompose over time.

Oxidant Screening

Attempts to determine the reaction order with respect to oxidant have been unsuccessful thus far as we have found no oxidant that is both soluble and competent under reaction conditions. Metal carboxylate oxidants, have proven to be competent oxidants in this system, but are relatively

insoluble in 1,2-dichloroethane. The benzoin derivatives in the top row of figure 8 as well as the hypervalent iodine oxidants shown in the bottom row were soluble in 1,2-dichloroethane but were incompetent oxidants under reaction conditions (Table S6).

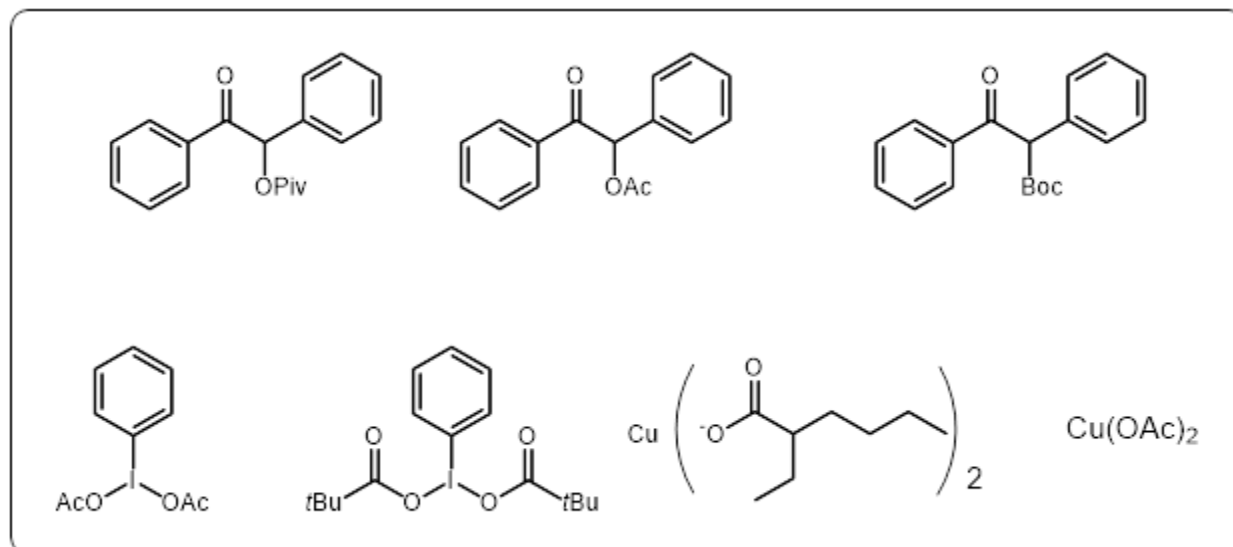


Figure 10. Oxidants tested for solubility and viability under reaction conditions

Controls (Role of Carboxylates)

Additionally, several reactions were run to assess the viability of this reaction with monomeric rhodium catalysts without metal carboxylate sources. Reactions run with benzoyl peroxide as the oxidant did generate a low yield of the desired amination product but led to decomposition of the olefin at a much faster rate. The use of diisopropylethylamine (DIPEA) in all cases shut down reactivity, possibly due to the ability of DIPEA to competitively bind to rhodium. Silver tetrafluoroborate proved to be unable to oxidize, even in the presence of catalytic amounts of carboxylate. These results in combination with the results from the oxidant screen suggest that a superstoichiometric equivalent of carboxylate is necessary in order to turn over the reaction, and that catalytic amounts of carboxylate are not sufficient to achieve the same effect.

Catalyst	Oxidant	Additive	Result
RhCp*(OAc) ₂ ^a	AgBF ₄ ^b	None	No desired product
RhCp*(OAc) ₂ ^a	(BzO) ₂ ^c	None	Olefin decomposition
RhCp*(OAc) ₂ ^a	(BzO) ₂ ^c	DIPEA ^d , AgBF ₄ ^e	No desired product
RhCp*(OAc) ₂ ^a	AgOAc	AgBF ₄ ^e	5.4 ± 0.1 x10 ⁻⁶ (mol/s) product formation
[RhCp*(MeCN) ₃]SbF ₆ ^a	AgBF ₄ ^b	None	Trace product
[RhCp*(MeCN) ₃]SbF ₆ ^a	AgBF ₄ ^b	DIPEA ^d	No desired product
[RhCp*(MeCN) ₃]SbF ₆ ^a	(BzO) ₂ ^c	None	Olefin decomposition
[RhCp*(MeCN) ₃]SbF ₆ ^a	(BzO) ₂ ^c	AgBF ₄ ^e	Olefin decomposition

Table 1. Reaction screen with monomeric rhodium pre-catalysts. [1]=0.2 M, [2]=0.5 M, in DCE at 60°C. ^a[Rhodium]=0.012 M. ^b[AgBF₄]=0.42 M. ^c[(BzO)₂]=0.22 M. ^d[DIPEA]=0.42M. ^e[AgBF₄]=0.024 M

Stoichiometric π -allyl Complex Reactions¹⁷

To elucidate more information on the mechanism of this transformation, RhCp* π -allyl complex **4** (Figure 11) was synthesized and subjected to various reaction conditions (Table 2). In the presence of nucleophile **2** without any additional additives, only the complex **5** was recovered. In the presence of a stoichiometric equivalent of oxidant we see consumption of the starting complex and formation of the aminated product **6** in less than 10% yield. Increasing the equivalents of the oxidant leads to further consumption of complex **4** with less than 10% yield of product **6**. In the presence of a stoichiometric carboxylate source we see consumption of complex **4**, but no formation of the desired product. Only in the presence of both an oxidant and a carboxylate source is the significant formation of product **6** observed. These results suggest that both an oxidant and a carboxylate source are necessary to drive the reaction.

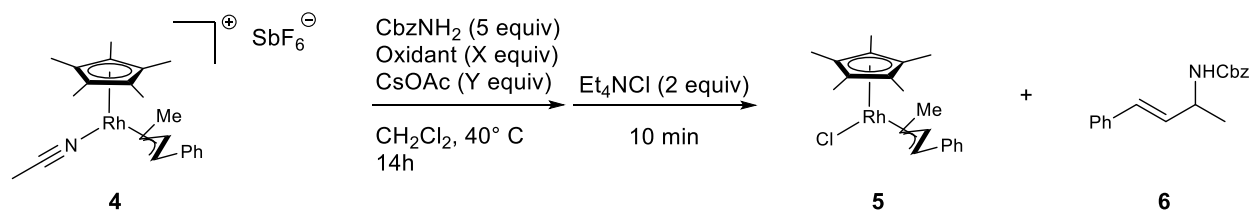


Figure 11. Stoichiometric amination of Rh π -allyl complex **4**

Oxidant (equiv)	CsOAc	Yield 5 ^a	Yield 6 ^a
--	--	92%	0%
AgSF_6 (1 equiv)	--	26%	7%
AgSF_6 (2 equiv)	--	0%	7%
--	1 (equiv)	30%	0%
AgSF_6 (2 equiv)	1 (equiv)	0%	29%

Table 2. Reactions with isolated Rh π -allyl complex **4**. ^aIsolated yields

Computational Studies¹⁸

Collaborations with computational chemists suggest two possible pathways for the allylic C–H amination of alkene **1**. The first pathway (Figure 12) suggests that concerted metalation deprotonation is the rate limiting step followed two steps later by a single electron oxidation to afford a Rh^{IV} species. This oxidation is subsequently followed by a reductive elimination to generate the aminated product and a Rh^{II} species that is then oxidized back to Rh^{III} . The second pathway (Figure 13) suggests that, unlike the first pathway, the reductive elimination step is rate limiting. Additionally, this pathway cycles between Rh^{III} and Rh^{I} oxidation states. According to the computational data, the first pathway is more kinetically accessible, and is the operative pathway at low temperatures (~ 40 – 60°). At elevated temperatures ($\sim 80^\circ\text{C}$ or higher) both reaction pathways may be accessible. In both cases, Ag^{I} is responsible for promoting the regeneration of the active rhodium catalyst.

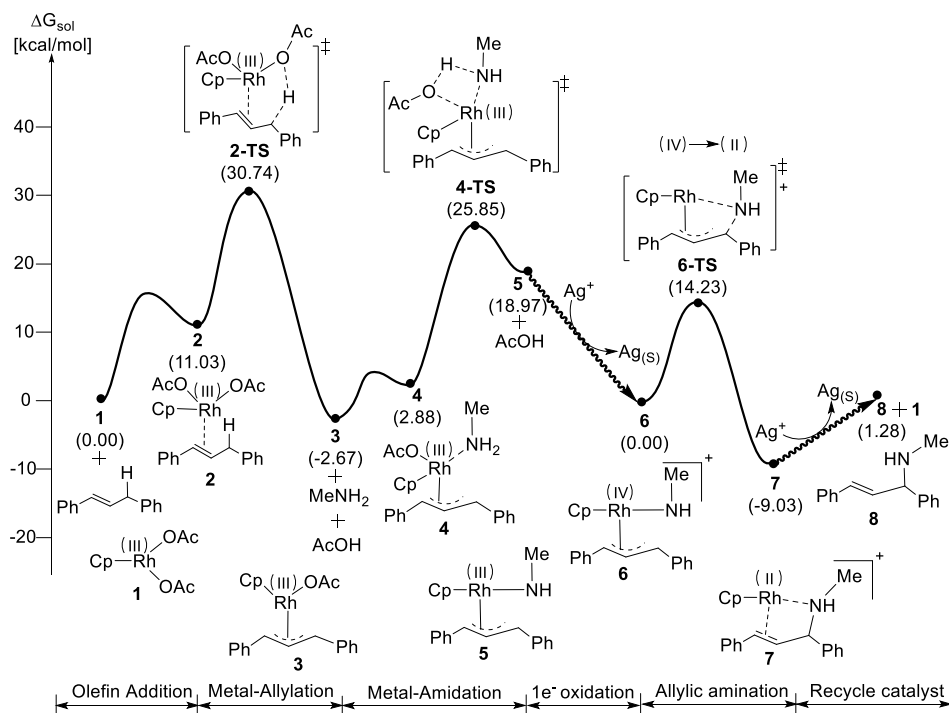


Figure 12. Computational studies depicting one possible pathway for the $\text{Rh}^{\text{II}}/\text{Rh}^{\text{IV}}$ catalyzed allylic C-H amination of alkene **1**. Computations were run with the following basis set: B3LYP-D3/cc-pVTZ(-f)/LACV3P**//B3LYP-D3/6-31G**/ LACVP** ($\epsilon = 9.08$). All energies are in kcal/mol.

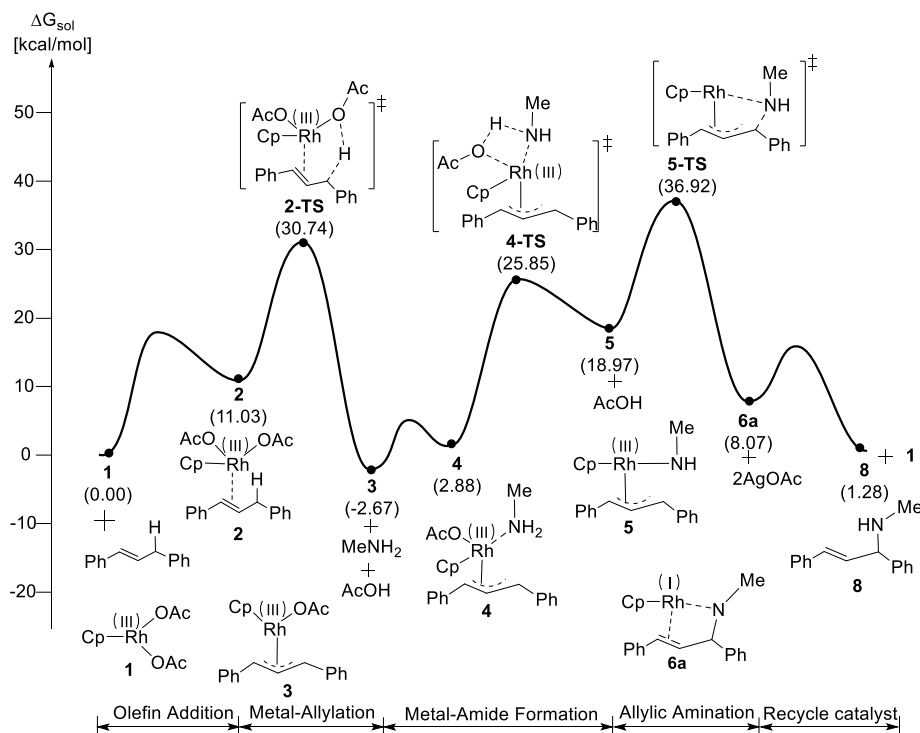
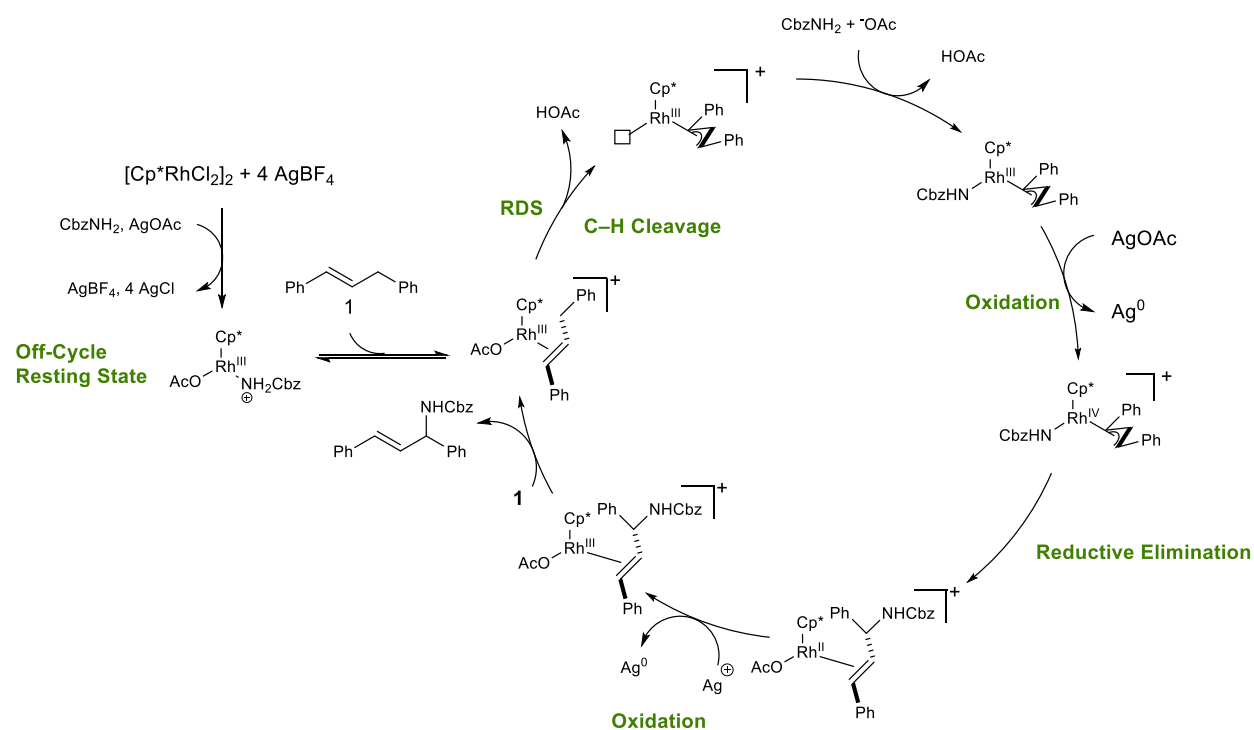


Figure 13. Computational studies depicting one possible pathway for the Rh^I/Rh^{III} catalyzed allylic C–H amination of alkene **1**. Computations were run with the following basis set: B3LYP-D3/cc-pVTZ(-f)/LACV3P**//B3LYP-D3/6-31G**/ LACVP** ($\epsilon = 9.08$). All energies are in kcal/mol.

With the information gathered from our kinetic studies, we propose the mechanism shown in Scheme 3. The mechanism begins silver tetrafluoroborate abstracting the chlorides from the rhodium pre-catalyst dimer, followed by the coordination of acetate and benzyl carbamate. At this point, benzyl carbamate must dissociate from the rhodium center in order to allow 1,3-diphenyl propene to coordinate. This step is consistent with the inhibition of the rate of formation of product **3**. This step is followed by rate limiting C–H cleavage to generate the rhodium π -allyl intermediate, ongoing collaborations with computational chemists suggest. Preliminary computational analysis

supports the coordination of benzyl carbamate to rhodium, followed by oxidation and subsequent reductive elimination to afford the aminated product and active rhodium catalyst.¹⁸

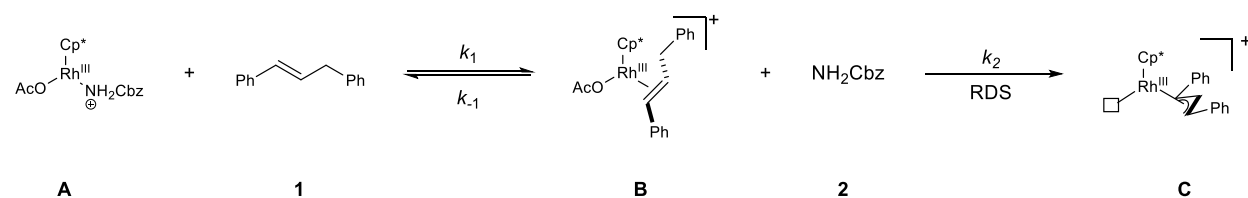
Scheme 3. Proposed reaction mechanism



Consider the catalytic cycle from the off-cycle resting state to the rate determining step

(Scheme 4):

Scheme 4. Pre-equilibrium and rate determining step



Because the conversion of **B** to **C** is a unimolecular process, the rate of formation of the product **C** is equal to:

$$\text{Rate} = k_2[\mathbf{B}]$$

(Equation 1)

In order to determine a rate law consistent with experimental and computational data a few assumptions must be made. Assuming the first step proceeds much faster than the second step, we can use the pre-equilibrium approximation to express $[\mathbf{B}]$ in terms of the equilibrium expression of the first step. The second assumption we make is that all of the rhodium in solution is taken up as either \mathbf{A} or \mathbf{B} (Equation 3). If k_2 is rate determining, this assumption should be valid as all other rhodium species should be transient.

$$K = \frac{[\mathbf{B}][\mathbf{2}]}{[\mathbf{A}][\mathbf{1}]}$$

(Equation 2)

$$[\mathbf{A}] = [\text{Rh}]_{\text{tot}} - [\mathbf{B}]$$

(Equation 3)

If equation 3 is substituted for $[\mathbf{A}]$ in the equilibrium expression, and then we subsequently solve for $[\mathbf{B}]$

we see:

$$K = \frac{[\mathbf{B}][\mathbf{2}]}{([\text{Rh}]_{\text{tot}} - [\mathbf{B}]][\mathbf{1}]}$$

(Equation 4)

$$[\mathbf{B}] = \frac{K[\text{Rh}]_{\text{tot}}[\mathbf{1}]}{K[\mathbf{1}] + [\mathbf{2}]}$$

(Equation 5)

This expression can then be substituted back into the initial rate law to afford the equation below:

$$\text{Rate} = k_2 \frac{K[\text{Rh}]_{\text{tot}}[\mathbf{1}]}{K[\mathbf{1}] + [\mathbf{2}]}$$

(Equation 6)

Which can then be rearranged to afford:

$$\text{Rate} = k_2[\text{Rh}]_{\text{tot}} \left(\frac{K[\mathbf{1}]}{K[\mathbf{1}] + [\mathbf{2}]} \right)$$

(Equation 7)

If the equilibrium constant K is small, the equilibrium strongly favors the formation of **A** and **1**. As K approaches 0, the $K[\mathbf{1}]$ factor in the denominator approaches zero and the fraction in parentheses can be approximated to

$$\frac{K[\mathbf{1}]}{[\mathbf{2}]}$$

(Equation 8)

Thus, if $K \ll 1$,

$$\text{Rate} = k_2[\text{Rh}]_{\text{tot}} \frac{K[\mathbf{1}]}{[\mathbf{2}]}$$

(Equation 9)

This rate expression is consistent with the experimental kinetic data as we see a first order dependence on $[\text{Rh}]_{\text{tot}}$ and $[\mathbf{1}]$, and a negative order dependence on $[\mathbf{2}]$. At first glance it would appear that this reaction proceeds in an overall first order fashion. However, because the concentration of rhodium remains constant throughout the reaction, the $[\text{Rh}]_{\text{tot}}$ term can be treated as a constant. Additionally, under the experimental conditions used to monitor the reaction the ratio of 1:2 does not change significantly, causing us to observe an overall zero-order reaction that comes from first order dependence on $[\mathbf{1}]$ and inverse order dependence on $[\mathbf{2}]$.

Conclusions and Future Directions

Although the complete kinetic profile of this reaction is not reported, this project provided important insight into the mechanism of this rhodium catalyzed allylic C–H amination of 1,2-disubstituted olefins. This project concluded that the reaction exhibits an overall pseudo-zero order kinetic profile, with first order dependence on both the catalyst and the olefin. Additionally, the reaction rate is inhibited by benzyl carbamate. The kinetic dependence on the oxidant has yet to be determined as no competent, soluble oxidant has been found yet.

This project is currently ongoing and there are two main objectives. The first objective is to find a soluble oxidant that is compatible with this system in order to see if there is any kinetic dependence on the oxidant. The second objective is to determine the kinetic isotope effect for C–H bond cleavage. The deuterated substrate of interest has already been synthesized and kinetic studies on this substrate will begin shortly.

Supplemental Information

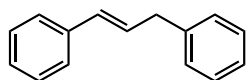
General Information

Materials: Reagents were purchased from commercial sources (Sigma Aldrich, Oakwood, Alfa Aesar, Fluka, and Fischer scientific) and were used as received, without further purification unless otherwise stated. DCE was purified via distillation over CaH_2 , and other anhydrous solvents were purified through alumina using a *Glass Contours* solvent purification system

Analysis: All ^1H NMR spectra were obtained on Varian NMR spectrometer operating at 400MHz for ^1H and 100 MHz for ^{13}C . All gas chromatograph spectra were taken on an Agilent Technologies 6850 series gas chromatograph equipped with a flame ionization detector and with a HP-1 column (30 m wide bore 0.32mm x 0.25 μm) manufactured by J&W. Synthesized compounds were purified with a Biotage flash column chromatography system with silica gel cartridges

Material Preparation

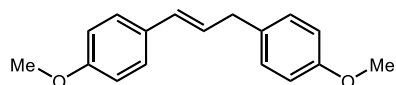
1,3-diphenyl propene¹⁹ (S1)



In a round bottom flask, phenylacetaldehyde (7.2g, 60.0mmol) potassium hydroxide pellets (3.6g, 64.0 mmol) and ethanol (200ml) were combined. The mixture was heated to 80°C and refluxed overnight. The mixture was concentrated *in vacuo*, dissolved in water and extracted three times with ethyl acetate. The organic layers were combined, washed with brine, dried over sodium sulfate, and concentrated *in vacuo*. The crude mixture was purified via flash chromatography

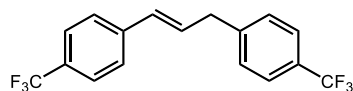
(Hex/EtOAc) to yield a viscous pale yellow liquid.(3.2 g, 55%) ; $^1\text{H NMR}$ (400 MHz, CDCl_3): δ 7.38 – 7.19 (m, 10H), 6.46 (d, $J = 15.6$ Hz, 1H), 6.47 (dt, $J = 15.6, 6.8$ Hz, 1H), 3.56 (d, $J = 6.4$ Hz, 2H)

(E)-4,4'-(Prop-1-ene-1,3-diyl)bis(methoxybenzene)²⁰ (S2)



To a sealed tube was added allyl acetate (200mg, 2.0 mmol), 4-iodoanisole (1.17g, 5.0 mmol), palladium acetate (45.0mg, 10 mol%), triethylamine (1.6g, 1.16mL, 8.0 mmol), tetrabutylammonium chloride (0.834g, 3.0 mmol), and acetonitrile (20mL). The mixture was stirred for 12 h at 120°C under an atmosphere of air. After 12 h, the reaction mixture was cooled to room temperature, diluted with diethyl ether, and washed with brine. The brine was subsequently extracted three times with diethyl ether, the organic layers were combined, dried over sodium sulfate, and concentrated *in vacuo*. The crude mixture was purified via flash chromatography To afford a white solid (188 mg,37%) $^1\text{H NMR}$ (400 MHz, CDCl_3) δ : 7.27 (t, $J = 7.5$ Hz, 2H), 7.15 (d, $J = 8.5$ Hz, 2H), 6.86-6.81 (m, 4H), 6.37 (d, $J = 15.8$ Hz, 1H), 6.24-6.16 (m, 1H), 3.78 (s, 6H); 3.46 (d, $J = 6.6$ Hz, 2H)

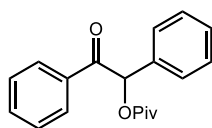
(E)-4,4'-(Prop-1-ene-1,3-diyl)bis(trifluoromethylbenzene)²¹ (S3)



To a sealed tube was added allyl acetate (200mg, 2.0 mmol), 4-iodobenzotrifluoride (1.36g, 5.0 mmol), palladium acetate (45.0mg, 10 mol%), triethylamine (1.6g, 1.16mL, 8.0 mmol),

tetrabutylammonium chloride (0.834g, 3.0 mmol), and acetonitrile (20mL). The mixture was stirred for 12 h at 120°C under an atmosphere of air. After 12 h, the reaction mixture was cooled to room temperature, diluted with diethyl ether, and washed with brine. The brine was subsequently extracted three times with diethyl ether, the organic layers were combined, dried over sodium sulfate, and concentrated *in vacuo*. The crude mixture was purified via flash chromatography to afford a white solid (198 mg, 30%) ¹H NMR (400 MHz, CDCl₃): δ : 7.51–7.46 (m, 4H), 7.36 (d, J=8.0 Hz, 2H), 7.27 (d, J= 8.0 Hz, 2H), 6.41 (d, J=16.0 Hz, 1H), 6.38–6.32 (m, 1H), 3.50 (d, J=6.0 Hz, 2H)¹¹

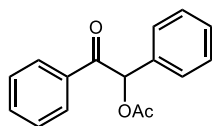
2-Oxo-1,2-diphenylethyl pivalate²² (S4)



To a flame dried flask under an inert atmosphere was added benzoin (0.848g, 4.0 mmol) and pyridine (5.0 mL). To this mixture was added pivaloyl chloride (0.74 mL, 6.0 mmol) dropwise. The reaction mixture stirred for 16 h at room temperature under an inert atmosphere. After 16 h, the mixture was concentrated *in vacuo*, and re-dissolved in diethyl ether. The ether solution was washed three times each with 1N HCl in water, a saturated sodium bicarbonate

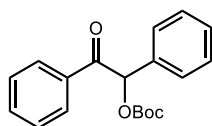
solution, and brine. The organic layer was then dried with sodium sulfate and the solvent was removed in vacuo to afford a white solid (0.912g, 77% yield) ^1H NMR (400 MHz, CDCl_3) δ : 7.93-7.96 (2H, m), 7.46-7.54 (3H, m), 7.31-7.43 (5H, m), 7.31-7.43 (5H, m), 6.80 (1H, s), 1.29 (9H, s)

2-Oxo-1,2-diphenylethyl acetate²² (S5)



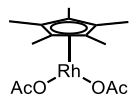
To a flame dried flask under an inert atmosphere was added benzoin (1.0g, 5.0 mmol) and pyridine (12.0 mL). To this mixture was added acetic anhydride (0.70 mL, 2.5 mmol) dropwise. The reaction mixture stirred for 16 h at room temperature under an inert atmosphere. After 16 h, the mixture was concentrated *in vacuo*, and re-dissolved in diethyl ether. The ether solution was washed three times each with 1N HCl in water, a saturated sodium bicarbonate solution, and brine. The organic layer was then dried with sodium sulfate and the solvent was removed in vacuo and the crude mixture was purified via flash chromatography to afford a white solid (g, 75% yield) ^1H NMR (400 MHz, CDCl_3) δ :7.92-7.96 (2H, m), 7.51-7.55 (1H, m), 7.32-7.42 (5H, m), 6.87 (1H, s), 2.21 (3H, s)

2-(*tert*-Butoxycarbonyloxy)-1,2-diphenylethanone²² (S6)



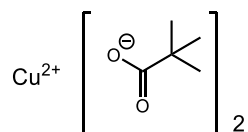
To a solution of benzoin (0.637g, 3.0mmol) and zinc acetate (55.0 mg, 0.3 mmol) in dichloromethane (3.0 mL) was added Boc anhydride (0.720g, 0.758mL, 3.3 mmol). The reaction mixture was heated to 40°C and was refluxed for 19 h. After 19 h, the reaction mixture was diluted with dichloromethane and washed with water three times. The solvent was removed *in vacuo* and the crude mixture was purified via flash chromatography to afford a pale-yellow crystal (814 mg, 2.61 mmol, 81% yield) ¹H NMR (400 MHz, CDCl₃) δ : 7.30-7.50 (m, 8 H) 7.92-7.96 (m 2 H.), 6.70 (s, 1 H), 1.49 (s, 9 H) ppm

Cp*Rh(OAc)₂²³ (S7)



In a nitrogen filled glove box, a [RhCp*Cl₂]₂ (0.0473g, 0.077mmol) and silver acetate (0.0625g, 0.37 mmol) were added to a 7 mL vial. The vial was equipped with a septum cap and removed from the box. Dry dichloromethane (1.54 mL) was added via syringe and the reaction was left to stir under an inert atmosphere at room temperature for 72 h. The crude reaction mixture was filtered through diatomaceous earth and washed with more dichloromethane. The solvent was evaporated *in vacuo* to afford a red-orange solid (47.0 mg, 82% yield) H NMR (400MHz, CDCl₃) 1.68 (s, 15H), 1.93 (s, 6H) ppm

Copper (II) Pivalate (S8)²⁵

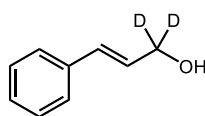


To a round bottom flask was added pivalic acid (1.12 g, 11 mmol, sodium hydroxide (0.4 g, 10 mmol), and 8 mL of deionized water. The mixture stirred at room temperature under an air

atmosphere. After 1 h, the mixture was filtered and the filtrate was added to a solution of $\text{Cu}(\text{NO}_3)_2$ (1.2 g, 5 mmol) in 8 mL of water. The resulting mixture stirred at room temperature for an additional hour, after which the mixture was filtered, and the precipitate was washed with additional water to afford a blue solid

Preparation of Deuterated Olefin for Kinetic Isotope Effect Studies

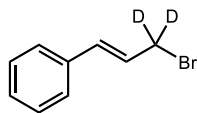
(E)-1,1-dideutero-3-phenylprop-2-en-1-ol(98.5%D)²⁶ (S9)



In a nitrogen filled glove box lithium aluminum deuteride (98%D) (230.7 mg, 5.5 mmol, 0.55 equiv) and a stir bar were added to a 50 mL round bottom flask. The flask was subsequently sealed with a septum and removed from the glove box. Anhydrous THF (16 mL) was added via syringe, and the resulting mixture was cooled to 0°C in a brine/ice bath. Ethyl cinnamate (1.68 mL, 10.0 mmol) was added dropwise over the course of 5 minutes while stirring rapidly. The reaction mixture was then allowed to stir for an hour. After 1 h, the reaction mixture was re-cooled to 0°C in a brine/ice bath and was quenched with the dropwise addition of deionized water (0.24 mL), followed by 1M aqueous sodium hydroxide (0.24 mL), and additional deionized water (0.72 mL) while stirring rapidly. The quenched mixture was allowed to stir for 30 minutes, after which it was diluted with diethyl ether (16 mL) and filtered through a plug of diatomaceous silica, eluting with additional diethyl ether. The filtrate was then washed with 1M aqueous hydrochloric acid. The aqueous layer was then extracted twice with additional diethyl ether. The combined organic layers were washed with brine, dried over sodium sulfate, concentrated *in vacuo*, and purified via flash chromatography to afford a clear oil (610 mg, 4.5 mmol, 45% yield, 98.5%D) (Hex/Et₂O) ¹H

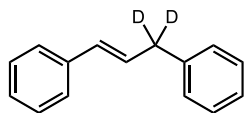
NMR (400 MHz, CDCl₃) δ = 7.39 (d, J = 7.6 Hz, 2 H), 7.33 (t, J = 7.6 Hz, 2 H), 7.21 (t, J = 7.6 Hz, 1 H), 6.63 (d, J = 15.6 Hz, 1 H), 6.37 (d, J = 15.6 Hz, 1 H) ppm

(E)-(3-bromoprop-1-en-1-yl-3,3-d₂)benzene(98.5%D)²⁷ (S10)



S9 (500 mg, 3.67 mmol, 2.0 equiv) and diethyl ether (5.3 mL) were added to a round bottom flask. The reaction mixture was cooled to 0°C in a brine/ice bath and PBr₃ (0.174 mL, 1.84 mmol, 1.0 equiv) was added via syringe. The reaction mixture was warmed to room temperature and was allowed to stir for an additional 24 h. After 24 h, the reaction was quenched with the addition of a saturated aqueous solution of ammonium chloride. The aqueous layer was extracted three times with diethyl ether, and the combined organic layers were dried with MgSO₄ and concentrated *in vacuo* and purified via flash chromatography to afford a yellow residue (436 mg, 2.54 mmol, 69% yield, 98.5% D)) ¹H NMR (400 MHz, CDCl₃) δ 7.40-7.24 (m, 5H), 6.64 (d, J =15.6 Hz, 1H), 6.39 (d, J =15.6 Hz, 1H) ppm

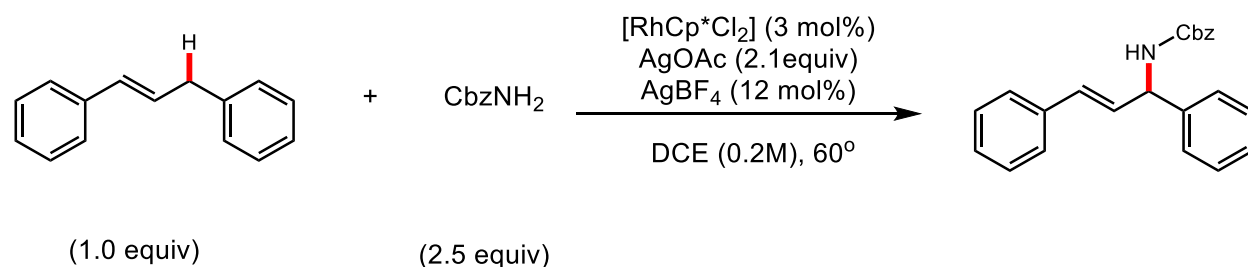
(E)-(prop-1-ene-1,3-diyl-3,3-d₂)dibenzene(98.5%D)²⁸ (S11)



S10 (430 mg, 2.16 mmol, 1 equiv), phenylboronic acid (42 mg, 2.80 mmol, 1.3 equiv), potassium fluoride (190 mg, 3.24 mmol, 1.5 equiv), and Toluene:Water (10:1, 6.6 ml) were added to a round bottom flask. The resulting mixture stirred at 90°C for 18 h. After 18 h, the reaction mixture was treated with 1M hydrochloric acid, and the aqueous layer was extracted three times with dichloromethane. The combined organic layers were dried with MgSO₄, concentrated *in vacuo* and

the crude mixture was purified via column chromatography to afford a clear oil (210 mg, 1.05 mmol, 49%, 98.5% D) ^1H NMR (400 MHz, CDCl_3) δ 7.40 – 7.18 (m, 10H), 6.47 (d, $J = 15.8$ Hz, 1H), 6.36 (d, $J = 15.8$ Hz, 1H) ppm

Kinetic Studies Procedures



In a nitrogen filled glove box a stir bar, benzyl carbamate (194 mg, 1.28 mmol) and silver acetate (180 mg, 1.08 mmol) were added to a 7 mL vial. Silver tetrafluoroborate was added to a 4 mL vial and the rhodium catalyst was added to a separate 4mL vial. The vials were subsequently fitted with septum caps and removed from the glove box. The internal standard, nonane, was added to a volumetric flask followed by the addition of distilled 1,2-dichloroethane to create a ~0.1M solution. 2.3 mL of the solution was added to the 7mL vial and 1 mL of this solution was added to each of the 4mL vials to create stock solutions of silver tetrafluoroborate and the rhodium catalyst. 0.1mL of neat 1,3-diphenyl propene and 0.1mL from each of the stock solutions were added via syringe to the reaction vial, and the vial was placed in a heating block resting on a hot plate set to 60°C. Placing the vial in the heating block was considered the $t=0$ time point for kinetic analysis. Reaction progress was monitored by removing an aliquot of the reaction mixture (~50 μL). Each aliquot was taken using a fresh syringe (1mL) and a clean reusable needle. Each sample was worked up by filtering through diatomaceous silica using ethyl acetate as the eluent and then analyzed by gas chromatography equipped with a flame ionization detector. Helium was used as

the inert carrier gas, with a steady flow of 2.0 mL/min. The optimized temperature ramp began at a temperature of 40°C and was raised to a temperature of 300°C at a rate of 10°C/min. The temperature of the detector and injector were held at 250°C and 225°C respectively. Under this optimized protocol, 1,3-diphenyl propene, benzyl carbamate, and the aminated product eluted at $t=14.341$ min, $t=11.367$ min, and $t= 22.460$ min respectively

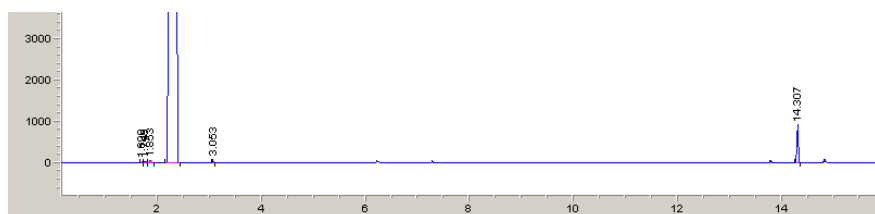


Figure S1. GC-FID of 1,3-diphenyl propene



Figure S2. GC-FID of Benzyl Carbamate

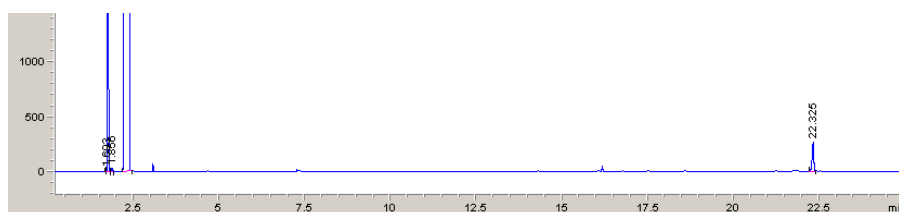


Figure S3. GC-FID of aminated product 3

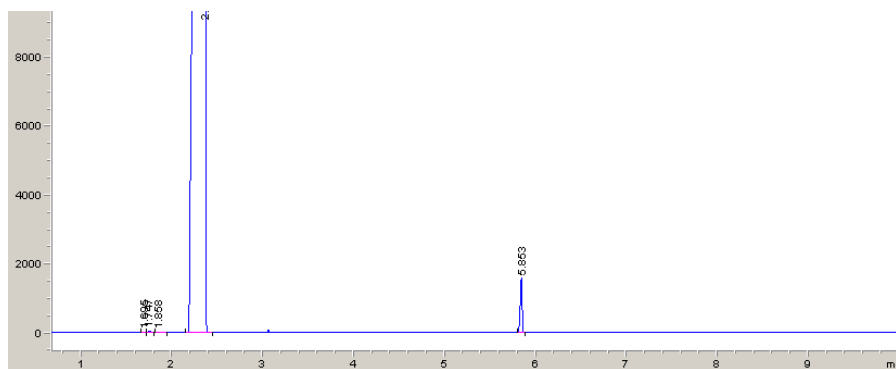


Figure S4. GC-FID of the internal standard

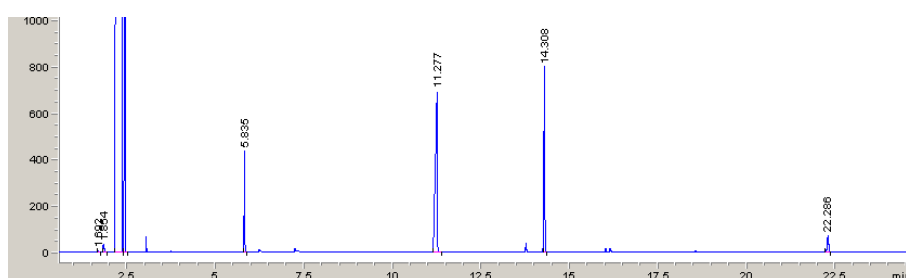
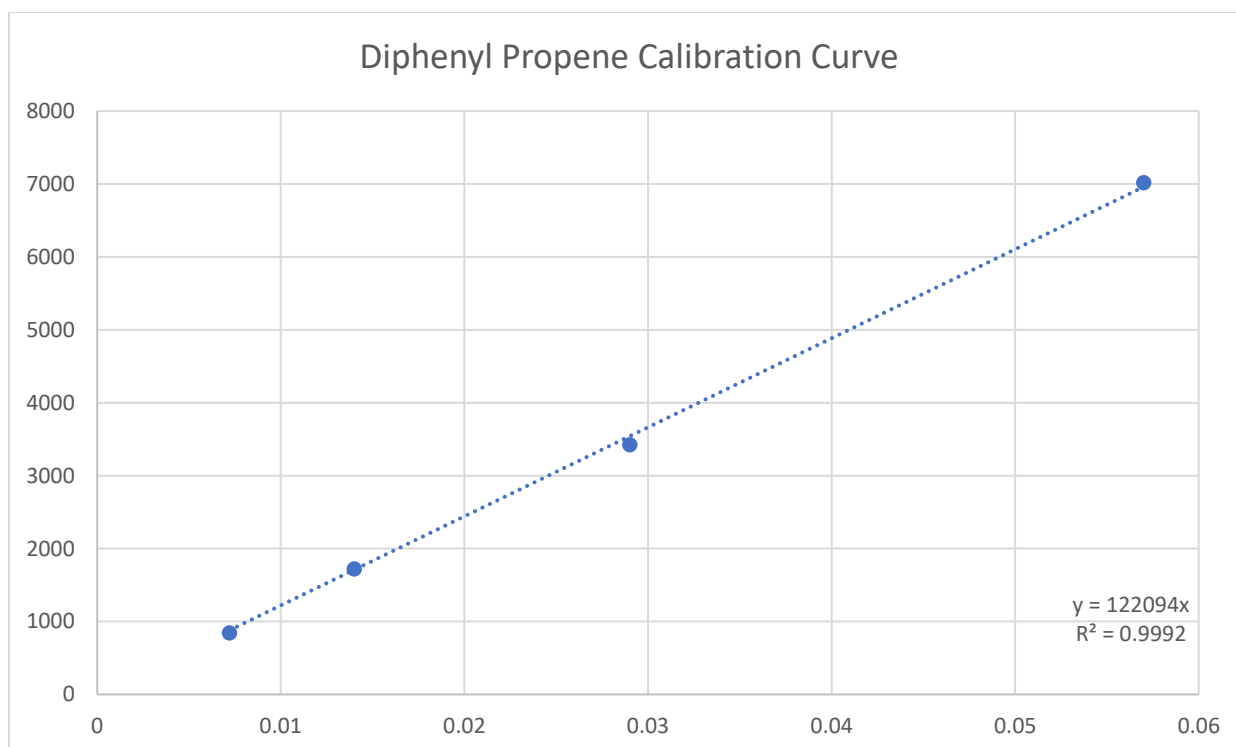
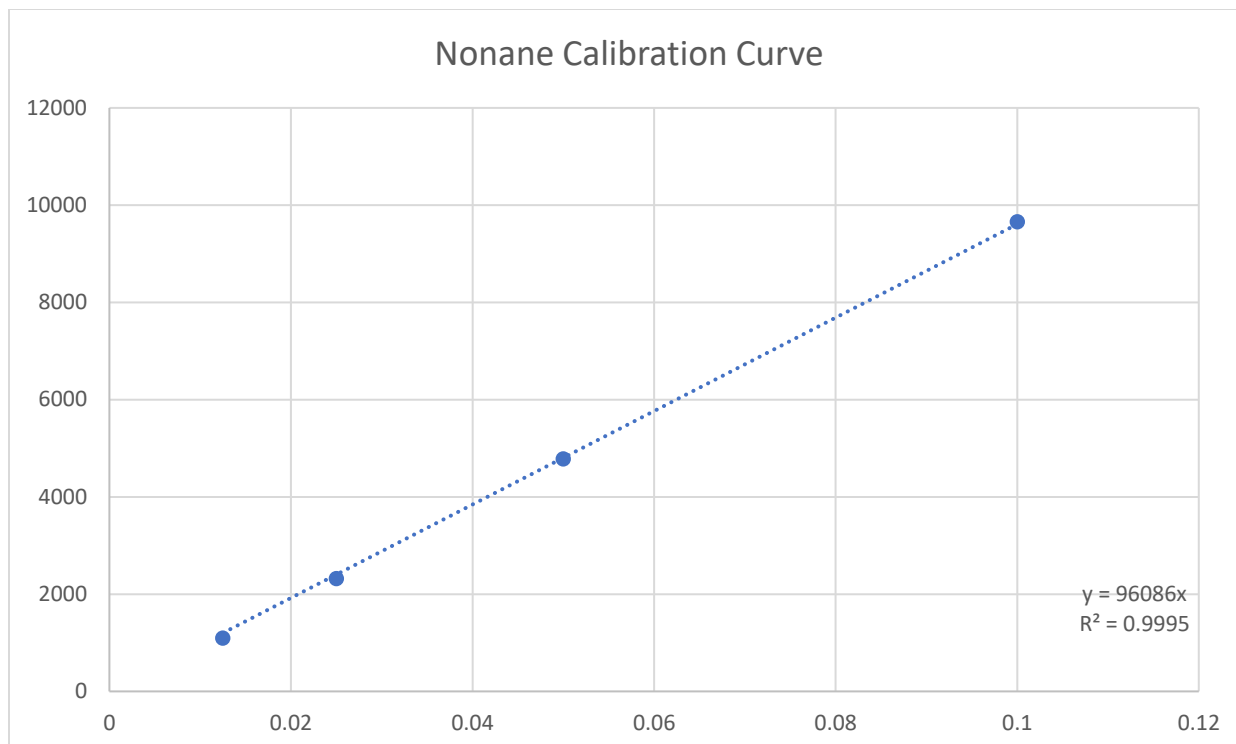
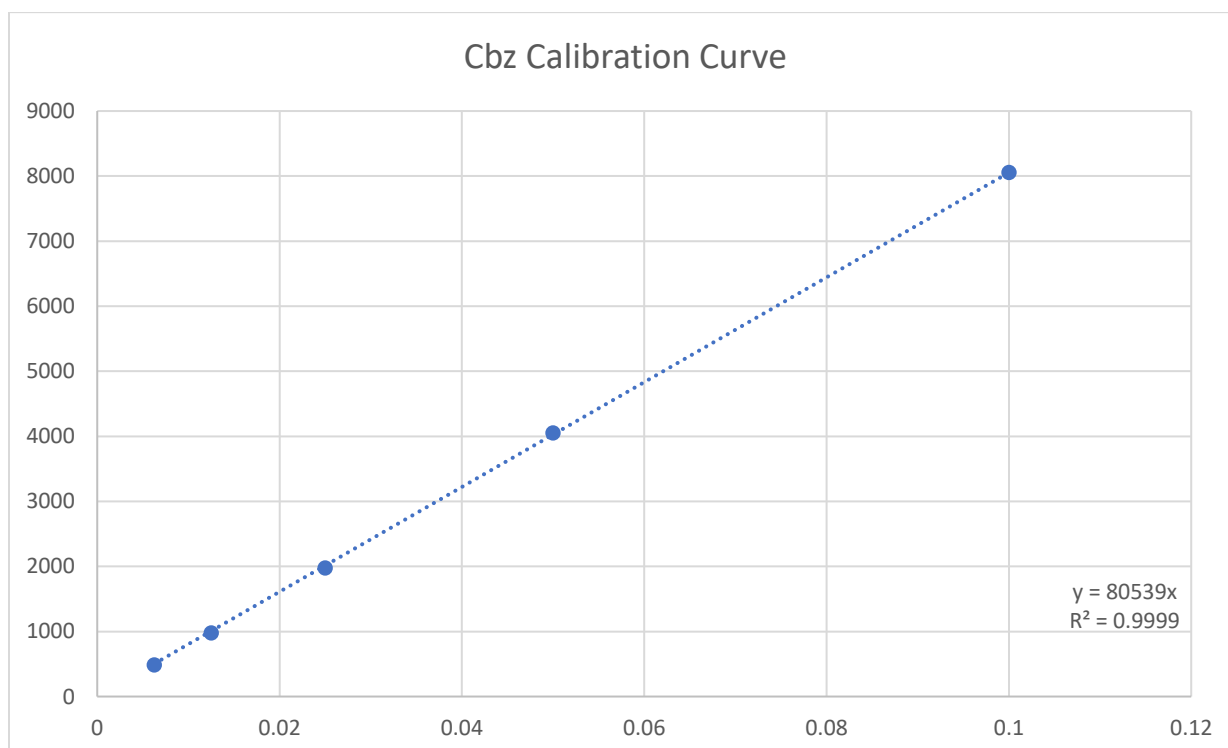
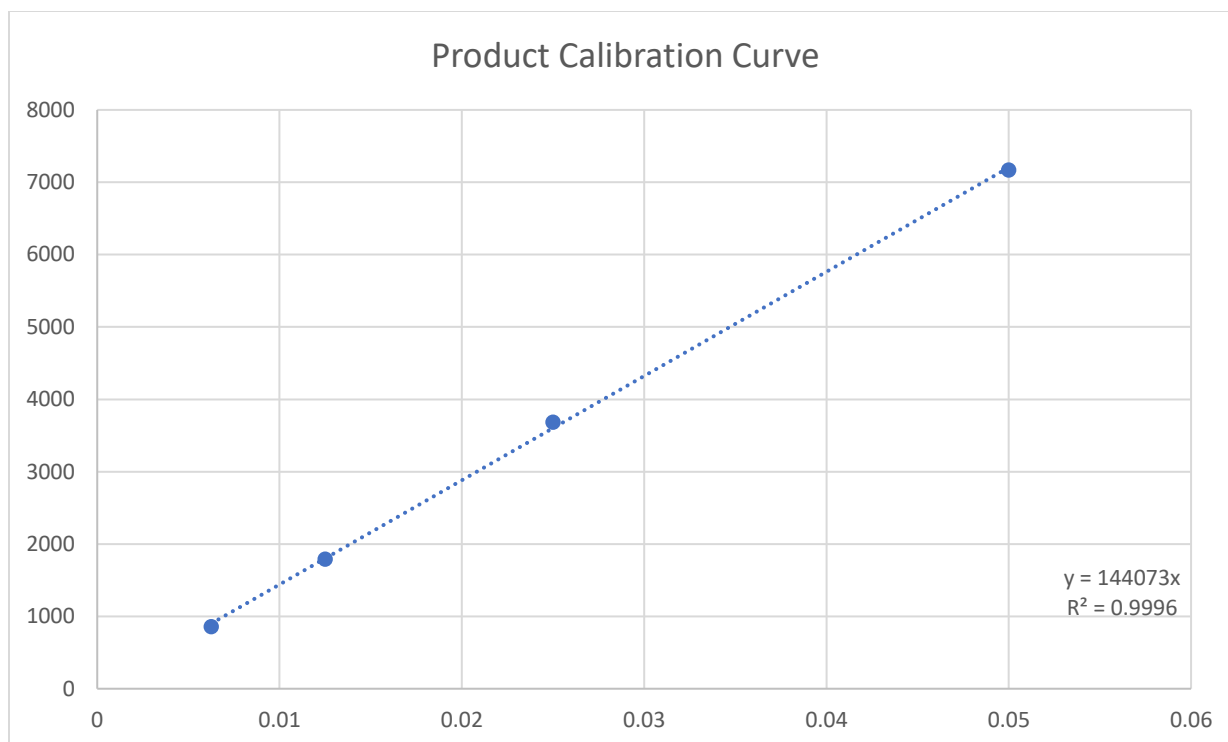


Figure S5. GC-FID of a running reaction as described in the kinetics studies procedure

Calibration of GC response ratios

To evaluate the relative responses of each component of the reaction, each compound was dissolved in ethyl acetate and diluted to several different known concentrations and the slopes of the resulting trend lines were compared





Substance	Slope	Response Ratio
1,3-diphenyl propene	122094	0.786984
Benzyl Carbamate	80539	1.193037
Nonane	96086	1
3	144073	0.666926

Table S1. Response factors of kinetically relevant species and response factor ratios relative to nonane

Kinetics Data

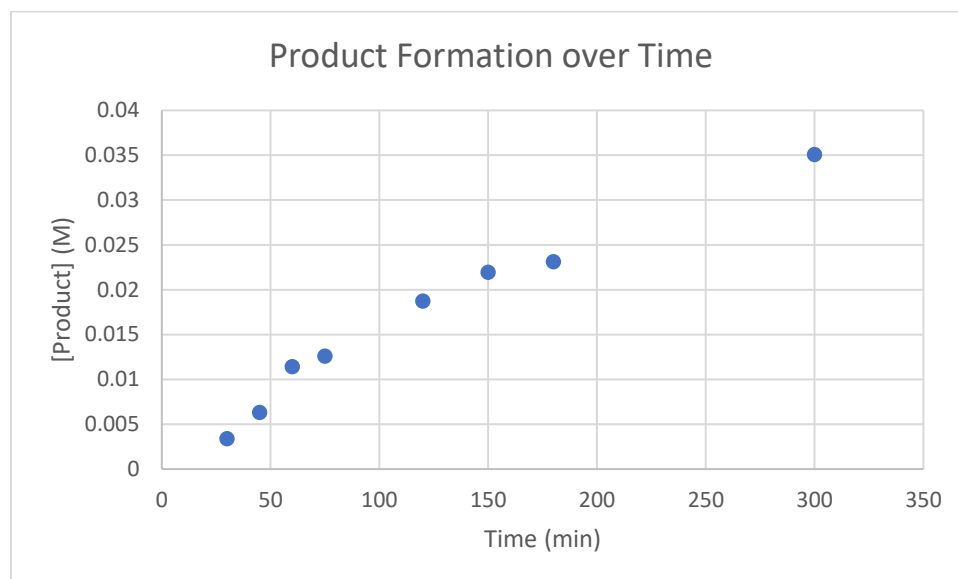


Figure S6. A representative plot of product formation over time under reaction conditions shown in Scheme 1. $[1]=0.2$ M, $[TsNH_2]=0.5$ M, $[AgOAc]=0.42$ M, $[AgBF_4]=0.008$ M, $[[RhCp^*Cl_2]_2]=0.002$ M

In Figure S5, it is difficult to determine the trend in product formation over time and as such it is unclear what the overall order of the reaction is. To address these issues, all future reactions were run with benzyl carbamate, a significantly more soluble nucleophile and reaction samples were filtered through diatomaceous earth instead of silica gel. Employing these changes yielded much clearer data, allowing for better interpretation and understanding of the reaction.

Order in catalyst experiments

Reaction order in catalyst studies were completed using general kinetics experimental procedure except with variations in concentration of $[\text{RhCp}^*\text{Cl}_2]_2$. See Figure 7a and 7b in the body

Experiment	[Catalyst] (M)	Reaction Rate (mol/s)
Control (No Catalyst)	0.00	0
Standard	0.002	$1.4 \pm 0.1 \times 10^{-06}$
2x Catalyst	0.004	$2.9 \pm 0.2 \times 10^{-06}$
3x Catalyst	0.006	$4.2 \pm 0.2 \times 10^{-06}$
4x Catalyst	0.008	$6.5 \pm 0.2 \times 10^{-06}$

Table S2. Global reaction rate dependence on [Rh catalyst]

Order in olefin experiments

Reaction order in these studies were completed using general kinetics experimental procedure except with variations in concentration of 1,3-diphenyl propene and 3x catalyst loading. See Figure 7c and 7d in the body

Experiment	[1,3-diphenyl propene] (M)	Reaction Rate (mol/s)
No Olefin	0.00	0.00
Standard	0.20	$4.3 \pm 0.1 \times 10^{-06}$
2x Olefin	0.40	$9.5 \pm 0.2 \times 10^{-06}$
3x Olefin	0.60	$1.19 \pm 0.03 \times 10^{-05}$

Table S3. Global reaction rate dependence on [olefin]

Order in nucleophile experiments

Reaction order in these studies were completed using general kinetics experimental procedure except with variations in concentration of benzyl carbamate. See Figure 7e and 7f in the body.

Experiment	[Benzyl carbamate] (M)	Reaction Rate (mol/s)
0.5x Nucleophile	0.25M	$1.93 \pm 0.02 \times 10^{-06}$
Standard	0.50M	$1.40 \pm 0.05 \times 10^{-06}$
2.0x Nucleophile	1.00 M	$2.5 \pm 0.3 \times 10^{-07}$

Table S4. Global reaction rate dependence on [nucleophile]

Additional reactions were run with variations in the concentration of benzyl carbamate with 3x catalyst loading

Experiment	[Benzyl carbamate] (M)	Reaction Rate (mol/s)
0.5x Nucleophile	0.25M	$6.1 \pm 0.2 \times 10^{-06}$
1.5x Nucleophile	0.75M	$1.2 \pm 0.1 \times 10^{-06}$
2.0x Nucleophile	1.00M	$3.9 \pm 0.3 \times 10^{-07}$

Table S5. Global reaction rate dependence on [nucleophile]

Order in Halide Scavenger experiments

Reactions run to determine order with respect to AgBF_4 were run using the general kinetics procedure except with variation of concentration of AgBF_4

Experiment	$[\text{AgBF}_4]$ (M)	Reaction Rate (mol/s)
None	0	0
0.25x Halide Scavenger	0.006	$2.3 \pm 0.1 \times 10^{-07}$
0.33x Halide Scavenger	0.008	$4.2 \pm 0.2 \times 10^{-06}$
0.5x Halide Scavenger	0.012	$1.4 \pm 0.1 \times 10^{-06}$
0.75x Halide Scavenger	0.018	$1.5 \pm 0.1 \times 10^{-06}$
Standard	0.024	$1.40 \pm 0.05 \times 10^{-06}$
2x Halide Scavenger	0.048	$6.9 \pm 0.2 \times 10^{-06}$

Table S6. Global reaction rate dependence on [Halide Scavenger]

Oxidant Screening Experiments

Reactions were completed using general kinetics procedure except with various oxidants (See Figure 8 for oxidant numbering)

[DPP]	[CbzNH ₂]	[AgBF ₄]	[Rh catalyst]	Oxidant	Rate (mol/s)
0.20	0.50	0.024	0.006	1	0
0.20	0.50	0.024	0.006	2	0
0.20	0.50	0.024	0.006	3	0
0.20	0.50	0.024	0.006	4	0
0.20	0.50	0.024	0.006	5	0
0.20	0.50	0.024	0.006	6	$6.5 \pm 0.2 \times 10^{-06}$
0.20	0.50	0.024	0.006	7	$1.64 \pm 0.02 \times 10^{-06}$

Table S7. Oxidant screening reactions, DPP=1,3-diphenyl propene. 1=2-Oxo-1,2-diphenylethyl pivalate, 2=2-Oxo-1,2-diphenylethyl acetate, 3= 2-(*tert*-Butoxycarbonyloxy)-1,2-diphenylethanone, 4= (Diacetoxyiodo)benzene, 5= Bis(*tert*-butylcarbonyloxy)iodobenzene, 6=copper 2-ethylhexanoate, 7= copper acetate

Control (Role of Carboxylates) Experiments

These experiments were run using the general kinetics procedure except with the following changes listed below the table

Catalyst	Oxidant	Additive	Result
RhCp*(OAc) ₂ ^a	AgBF ₄ ^b	None	No desired product
RhCp*(OAc) ₂ ^a	(BzO) ₂ ^c	None	Olefin decomposition
RhCp*(OAc) ₂ ^a	(BzO) ₂ ^c	DIPEA ^d , AgBF ₄ ^e	No desired product
RhCp*(OAc) ₂ ^a	AgOAc	AgBF ₄ ^e	5.4 ± 0.1 x10 ⁻⁶ (mol/s) product formation
[RhCp*(MeCN) ₃]SbF ₆ ^a	AgBF ₄ ^b	None	Trace product
[RhCp*(MeCN) ₃]SbF ₆ ^a	AgBF ₄ ^b	DIPEA ^d	No desired product
[RhCp*(MeCN) ₃]SbF ₆ ^a	(BzO) ₂ ^c	None	Olefin decomposition
[RhCp*(MeCN) ₃]SbF ₆ ^a	(BzO) ₂ ^c	AgBF ₄ ^e	Olefin decomposition

Table S8. Reaction screen with monomeric rhodium precatalysts, [1]=0.2 M, [2]=0.5 M, in DCE at 60°C. ^a[Rhodium]=0.012 M. ^b[AgBF₄]=0.42 M. ^c[(BzO)₂]=0.22 M. ^d[DIPEA]=0.42M. ^e[AgBF₄]=0.024 M

References

1. P. Muller and C. Fruit, *Chem. Rev.*, **2003**, 103, 2905–2920.
2. Trost, B.M.; Vranken, D.L.V. *Chem. Rev.*, **1996**, 96, 395–422.
3. Grange, R.L.; Clizbe, E.A.; Evans, P.A. *Synthesis* **2016**, 48, 2911–2968
4. Liang, X.; Zhang, T.-Y.; Zeng, X.-Y.; Zheng, Y.; Wei, K.; Yang, Y. R. *J. Am. Chem. Soc.* **2017**, 139, 3364
5. G. Dequierez, V. Pons and P. Dauban, *Angew. Chem., Int. Ed.*, **2012**, 51, 7384–7395
6. Shibata, Y. and Tanaka, K., *Angew. Chem. Int. Ed.* **2011**, 50, 10917 – 10921
5. Chen, M.S. and White, M.C., *J. Am. Chem. Soc.*, **2004**, 126, 1346– 1347.
6. Trost, B.M. *Acc. Chem. Res.*, **1980**, 13,385–393.
7. (a) H. M. L. Davies and J. R. Manning, *Nature*, **2008**, 451, 417–424; (b) S. Fantauzzi, A. Caselli and E. Gallo, *Dalton Trans.*, **2009**, 5434–5443; (c) H. Lu and X. P. Zhang, *Chem. Soc. Rev.*, **2011**, 40, 1899–1909
8. Chen, M.S. and White, M.C., *J. Am. Chem. Soc.*, **2004**, 126, 1346–1347. [b] Covell, D.J. and White, M.C., *Angew. Chem. Int. Ed.*, **2008**, 47, 1-5. [c] Gormisky, P.E. and White, M.C., *J. Am. Chem. Soc.*, **2011**, 133, 12584–12589.
9. Cochet T., Bellosta, V., Roche, D., Ortholand, J., Greiner, A., and Cossy, J.; *Chem. Commun.*, **2012**, 48, 10745-10747.
10. Shibata, Y. and Tanaka, K., *Angew. Chem. Int. Ed.* **2011**, 50, 10917 – 10921
11. Fukui, M.; Hoshino, Y.; Satoh, T.; Miura, M.; Tanaka, K. *Adv. Synth. Catal.* **2014**, 356,1638–1644
12. Shibata, Y.; Kudo, E.; Sugiyama, H.; Uekusa, H.; Tanaka, K.; *Organometallics* **2016**, 35, 1547–1552
13. Burman, S.J. and Blakey, B.S.; *Angew. Chem. Int. Ed.*, **2017**, 56, 13666-13669
14. Blackmond, D., *J. Am. Chem. Soc.*, **2015**, 137, 10852–10866
15. Reactions run by Robert Harris in the Blakey group, unpublished work
16. Calculations performed by Nafees Iqbal, Debashis Sahu, and Mu-Hyun Baik* at KAIST, unpublished work.
17. Yuan, Q., *Chem. Commun.*, **2015**, 51, 11834-11836
18. Liu, Y., *Org. Lett.*, **2011**, 13 (5), pp 1126–1129
19. Yao, B., *Adv. Synth. & Cat.* **2012**, 354(6), 1069-1076
20. Cutulic, S. *J. Org. Chem.*, **2009**, 74 (22), 8713–8718
21. Rovis, T. *J. Am. Chem. Soc.* 2014, 136, 2735
22. Xie, L. *Chem. Eur. J.* **2011**, 17, 13653-13656
23. Zhou, J-H. *J. Coord. Chem.* **2006**, 59 (2), 147-156
24. Jacobsen, E.; *ACS Cent. Sci.*, **2016**, 2 (6), 416–423
25. Strohmman, C.; *Angew. Chem. Int. Ed.*, **2017**, 56, 6232-6235
26. M. Ueda, K. Nishimura, R. Kashima, I. Ryu, *Synlett*, **2012**, 23, 1085-1089
27. Young, A.J; White, M.C., *J. Am. Chem. Soc.*, **2008**, 130, 14090–14091.
28. Chen, M.S.; Prabakaran, N.; Labenz, N.A.; White, M.C., *J. Am. Chem. Soc.*, **2005**, 127 (19), pp 6970–697.